Results in Physics 17 (2020) 103141

Contents lists available at ScienceDirect

Results in Physics

journal homepage: www.elsevier.com/locate/rinp

Strain uniformity footprint on mechanical performance and erosion-corrosion behavior of equal channel angular pressed pure titanium

Sh. Attarilar[a,b], F. Djavanroodi[c,d], O.M. Irfan[e,f], F.A. Al-Mufadi[e], M. Ebrahimi[b,g,*], Q.D. Wang[b,g]

[a] Department of Pediatric Orthopaedics, Xinhua Hospital Affiliated to Shanghai Jiao Tong University, School of Medicine, Shanghai, China
[b] State Key Laboratory of Metal Matrix Composites, School of Material Science and Engineering, Shanghai Jiao Tong University, Shanghai, China
[c] Mechanical Engineering Department, Prince Mohammad Bin Fahd University, Al Khobar 31952, Saudi Arabia
[d] Mechanical Engineering Department, Imperial College, London SW7 2AZ, UK
[e] Mechanical Engineering Department, Qassim University, Buraidah 51452, Saudi Arabia
[f] Mechanical Engineering Department, Beni Suef University, Beni-Suef 62764, Egypt
[g] National Engineering Research Center of Light Alloys Net Forming, School of Material Science and Engineering, Shanghai Jiao Tong University, Shanghai, China

ARTICLE INFO

Keywords:
Severe plastic deformation
Grain refinement
Tensile properties
Hardness distribution
Erosion-corrosion resistance
Material homogeneity

ABSTRACT

In this paper, the effect of equal channel angular pressing (ECAP) on microstructure, mechanical, and erosion-corrosion behavior of commercial pure (CP) titanium was investigated through experimental work. Four passes of ECAP processing at 400 °C was performed on CP titanium. The results showed that the homogeneous structure and coarse equiaxed grains of the initial annealed sample are transformed into the combination of UFG and NS with an average size of 750 nm and 85 nm, respectively. Also, ECAP pass numbers increase the fraction of high angle grain boundaries which improves the ductility of the processed sample. The highest hardness and strength improvement rate was observed after the first pass. Furthermore, the increasing rate of hardness and strength is gradually decreased at the subsequent passes and reached the steady-state level at the 4th pass. This is due to the balance between hardening by dislocations and twinnings accumulation and softening by recovery mechanisms. As a result, a uniform hardness distribution on both the cross-sectional and longitudinal planes is achieved. It was confirmed that erosion-corrosion resistance of the processed sample is enhanced due to the grain refinement, material homogeneity, and quick formation of a strong oxide bond layer on the surface.

Introduction

Titanium-based alloys are utilized in a number of engineering industries and medical applications due to the exceptional strength, superior superplastic, low elastic modulus, suitable corrosion resistance, and acceptable compatibility with the human tissues [1–5]. Turbines blades, marine structure, hydraulic systems, and especially, orthopedic, dental implants, etc. are few applications of Ti alloys, [6]. For example, the alloy of Ti-6Al-4 V corresponds to nearly 50% of the total production of titanium as the biomaterial. However, there are some reports about the possibility of toxicological effects of aluminum and vanadium elements due to the ion release from the metallic implant to the surrounding tissue [7,8]. This may cause complication such as peripheral neuropathy, osteomalacia, and Alzheimer's disease. A possible substitute can be pure titanium as a favorable metallic biomaterial if the low mechanical properties as compared to the alloyed conditions are improved.

Recently, severe plastic deformation methods are employed to improve mechanical properties of metals and alloys by means of grain refinement up to the levels of ultrafine grains (UFG) and even, nanocrystalline (NC) [9,10]. Until now, a large number of different SPD methods have been introduced, experimented, and studied including equal channel angular pressing [11], high-pressure torsion [12], planar twist channel angular extrusion [13], planar twist extrusion [14], constrained groove pressing [15], multi-directional forging [16], equal channel forward extrusion [17], friction stir processing [18], twist extrusion [19], accumulative roll bonding [20], cyclic extrusion compression [21], etc. [22,23]. Generally, in these methods, hydrostatic pressure is exerted on the material to generate a large magnitude of plastic strain; consequently, this leads to the UFG/NC samples having desirable mechanical properties without any considerable changes at their shape and dimensions. According to the previous studies [9,24–26], equal channel angular pressing (ECAP) is the most widely utilized technique for fabricating UFG/NC materials.

* Corresponding author at: National Engineering Research Center of Light Alloys Net Forming, School of Material Science and Engineering, Shanghai Jiao Tong University, Shanghai, China.
E-mail addresses: ebrahimi@sjtu.edu.cn, ebrahimi@maragheh.ac.ir (M. Ebrahimi).

https://doi.org/10.1016/j.rinp.2020.103141
Received 29 February 2020; Received in revised form 24 April 2020; Accepted 26 April 2020
Available online 30 April 2020

On the other hand, erosion-corrosion is a phenomenon that causes material loss due to a number of reasons. Generally, two mechanisms have been proposed to describe the erosion-corrosion behavior of materials [27,28]. The first mechanism is the degradation of the surface hardness due to corrosion. The other mechanism is the removal of a passive protective thin layer on the surface. On this subject, erosion-corrosion behavior of several UFG/NC materials has been investigated. Some studies on titanium have reported that the UFG/NC Ti exhibits higher corrosion resistance as compared to the coarse-grained (CG) condition. This is due to grain size reduction, resulting in the faster formation and stronger bond of passive films at the surface crystalline defects. On the other hand, other studies reported lower and or no significant improvement in the corrosion resistance of UFG/NC pure titanium in comparison with CG metal [27,29,30].

The erosion-corrosion behavior of the UFG/NC commercial pure titanium has not been thoroughly studied and understood despite the essential role of this property in different engineering and medical industry. The main focus of previous studies on the corrosion or erosion-corrosion behavior of UFG/NC was on the effect of grain size reduction and texture with no reference to the role of strain distribution uniformity. Hence, the current work addresses this issue and focuses on evaluating the role of strain distribution on the mechanical properties and tribological behavior of commercial pure titanium.

Materials and research methodology

A bar stock of commercial pure titanium (CP-Ti) with the purity of 99.2% was prepared in the form of an extruded rod with the 20 mm diameter and 80 mm length. The testing samples were made from both CG and UFG titanium samples. The UFG one was obtained after four passes of the ECAP process with the 90°-channel-angle and 17°-outer-corner-angle using route B_C at 400 °C ± 20. The ECAP process was conducted on cylindrical samples by means of two-half die made of H13 steel as shown in Fig. 1(a). Also, CP-Ti samples subjected to different ECAP passes are shown in Fig. 1(b). Prior to ECAP, the titanium samples were annealed at 710 °C for 2 h and then, furnace cooled. A hydraulic press of 160 tons capacity was employed to conduct the experiments with a ram speed of 3 mm/s. Moreover, molybdenum disulfide-based solid (MoS_2) lubricant was used in order to reduce the friction effect.

Microstructure evaluation was conducted by means of optical microscopy, electron transmission microscopy (TEM), and electron backscatter microscopy (EBSD) on the cross-section of the annealed and ECAP processed titanium samples. For this aim, all specimens were ground up to 5000 grit with silicon carbide grinding paper; afterward, they were polished with a diamond suspension and followed by a colloidal silica suspension for obtaining a mirror-like surface. Eventually, all the polished specimens were ultrasonically cleaned with butanol for 10 min. The thin foils for TEM observations were prepared by mechanical milling followed by electrolytic thinning by means of a solution of ethanol and perchloric acid at the temperature of 233 K and voltage of 30 V. The TEM analysis was carried out in a JEOL 200CX instrument with an acceleration voltage of 100 kV. Grain size also was measured using the linear intercept method. Also, EBSD measurements were performed at an accelerating voltage of 20 kV and a beam current of 200 mA. It should be mentioned that a step size of 0.40 μm was employed for the initial material (annealed condition) and 50 nm for the processed counterparts. All analysis of EBSD data was carried out using TSL-OIM software. Besides, the average grain size was measured by EBSD images using the area fraction vs grain size distribution chart.

The Vickers hardness (HV) measurement was performed according to the ASTM E92-04 standard using Zwick/Roell machine (Model ZHU250). The HV tests with loading magnitude of 200 gf and dwell time of 10 s were conducted on the as-received annealed sample and after each ECAP pass condition along the cross-section and longitudinal directions as illustrated in Fig. 2(a). The distance between measured points on the longitudinal direction and cross-section area was 3 mm and 4 mm, respectively. Each test was measured twice in order to ensure the reliability and validity of the results. Also, a torsion machine (model ND-W500) was utilized to conduct the torsional behavior in accordance with the ASTM A938 standard on the annealed and ECAPed samples as represented in Fig. 2(b). Besides, erosion-corrosion (E-C) performance of the processed titanium was carried out using a slurry-pot method according to the ASTM G119 standard. Simulated body fluid was utilized as a test medium. Details of the design, manufacturing, and application of slurry-pot tester were discussed elsewhere [27]. In order to assess the E-C resistance, the weight loss was determined by using a high-precision digital balance with 0.001 g accuracy. To identify the existence of any elements on the surface of the samples after the E-C test, JEOL-JSM-7800F-Prime scanning electron microscope equipped with an energy-dispersive spectroscope (EDS) was utilized. It is worth mentioning that three tests were performed for each condition and the average magnitude was reported. Table 1 lists the erosion-corrosion conditions of the aforementioned tests.

Results and discussion

Microstructure analysis

Grain refinement of CP titanium through imposing intense plastic strain by four passes ECAP process is shown in Figs. 3 and 4. As can be

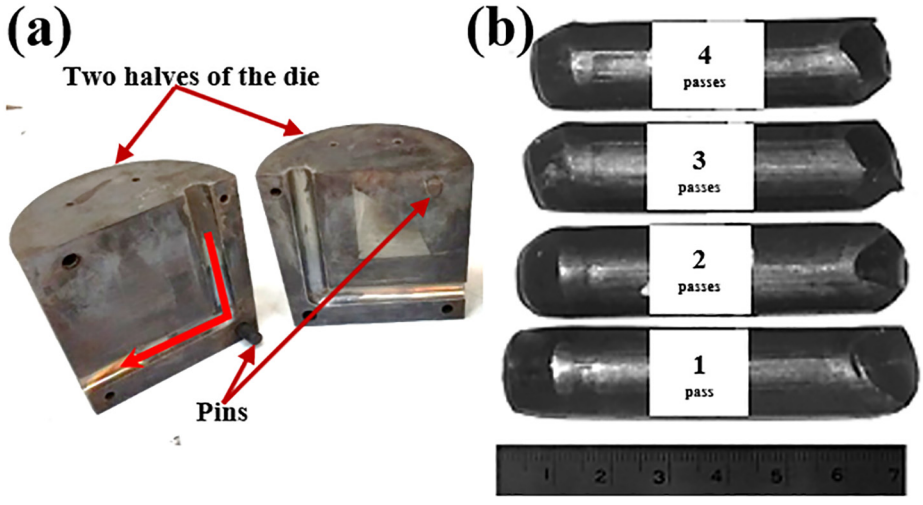

Fig. 1. (a) The utilized two-half ECAP die and (b) the processed titanium samples up to four passes.

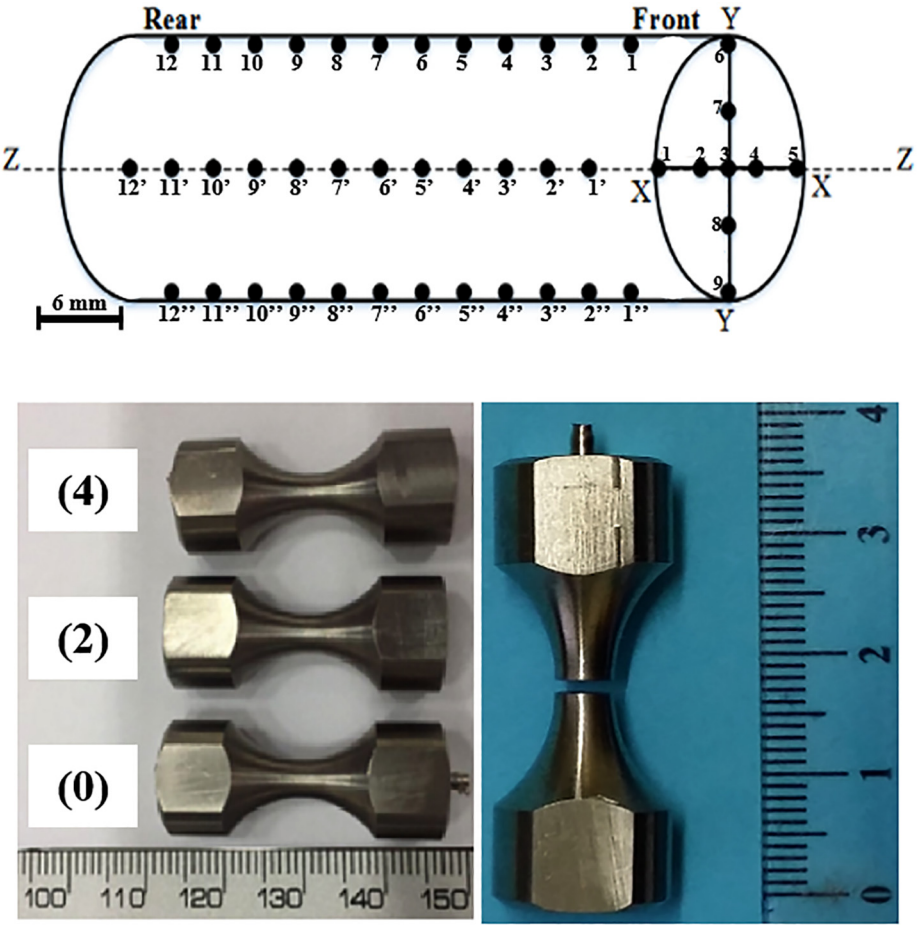

Fig. 2. (a) Schematic representation of recorded HV measurements on the cross-section and longitudinal planes and (b) the prepared samples of CP titanium before and after the torsion test.

Table 1
Summary of erosion-corrosion conditions for a slurry-pot method of as-received and processed titanium samples.

Experimental time, h	Linear velocity, m/s	Impacting angle, °
300 500 750 1000	5.4	45

observed in Fig. 3, annealing operation of the as-received material leads to the homogeneous and equiaxed microstructure. Accordingly, an average coarse grain size of about 20 μm was attained for this case. Employment of the ECAP process refines the microstructure of titanium samples into the combination of ultrafine-grained and nanostructured orders. Fig. 4(a) and (b) shows that the microstructures contain a considerable number of grains with different orientations; the variations of colors indicate orientation changes occurring inside the grains induced by severe plastic deformation. It is also clear from Fig. 4(c) that the microstructure consists of many recrystallized grains without dislocations marked by 1 (bright grains without any color changes), grains

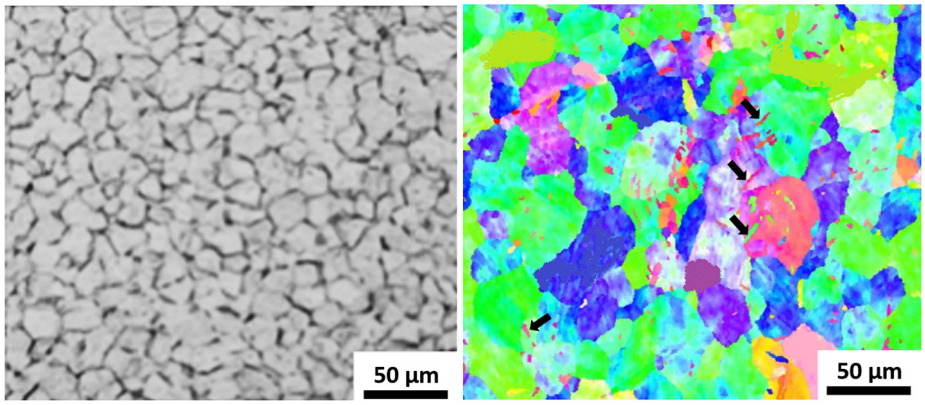

Fig. 3. Microstructure observation of CP titanium at the as-received annealed condition.

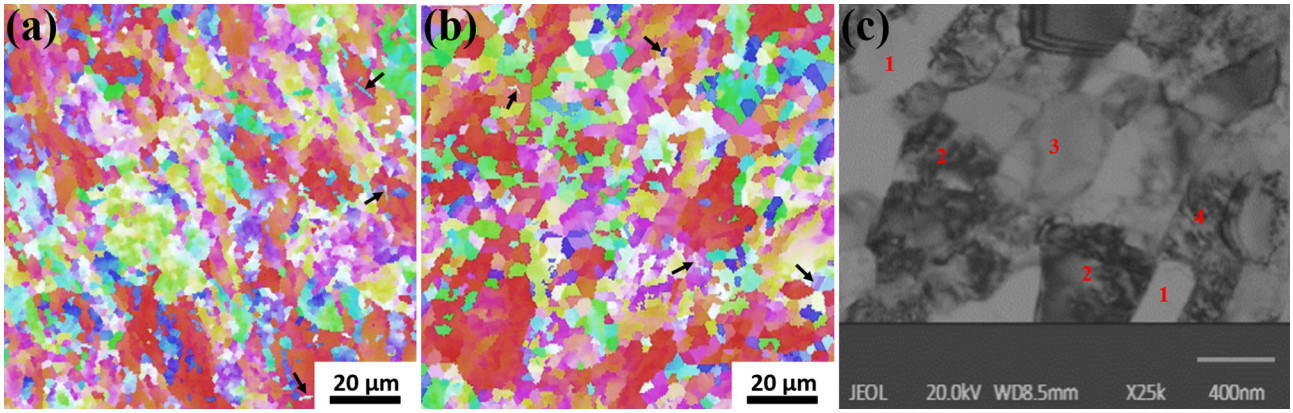

Fig. 4. Microstructure observation of CP titanium (a) after the second pass, (b) and (c) after the fourth pass of the ECAP process.

with various dislocations densities marked by 2 (grains with bright and dark color characteristics), subgrain cell structures with low angle grain boundaries marked by 3, next to some elongated new grains marked by 4. The average grain size of the titanium sample after the second and fourth passes of the ECAP process is about 1.35 and 1.09 μm; however, there are several ultrafine grains in the range of 400–500 nm and even many nanostructures with the order of 100 nm.

Fig. 5(a) and (b) shows the grain size distribution and the area fraction of grain sizes after applying two and four passes of ECAP process. The grain size distribution indicates a great deal of grain refinement of pure titanium by the employment of the ECAP process. In Fig. 5(a) and (b), the distribution of grain sizes shows the multimodal curve, indicating the nonhomogeneous microstructure formation through ECAP application. Also, as seen in Fig. 5(c) and (d), the amount of high angle grain boundaries (HAGBs) fraction is increased from 46% for the two-pass sample to about 50% for the four-pass sample. It is worth mentioning that the amount of medium angle grain boundaries (misorientation in the range of 10 to 15°) which is an indication of

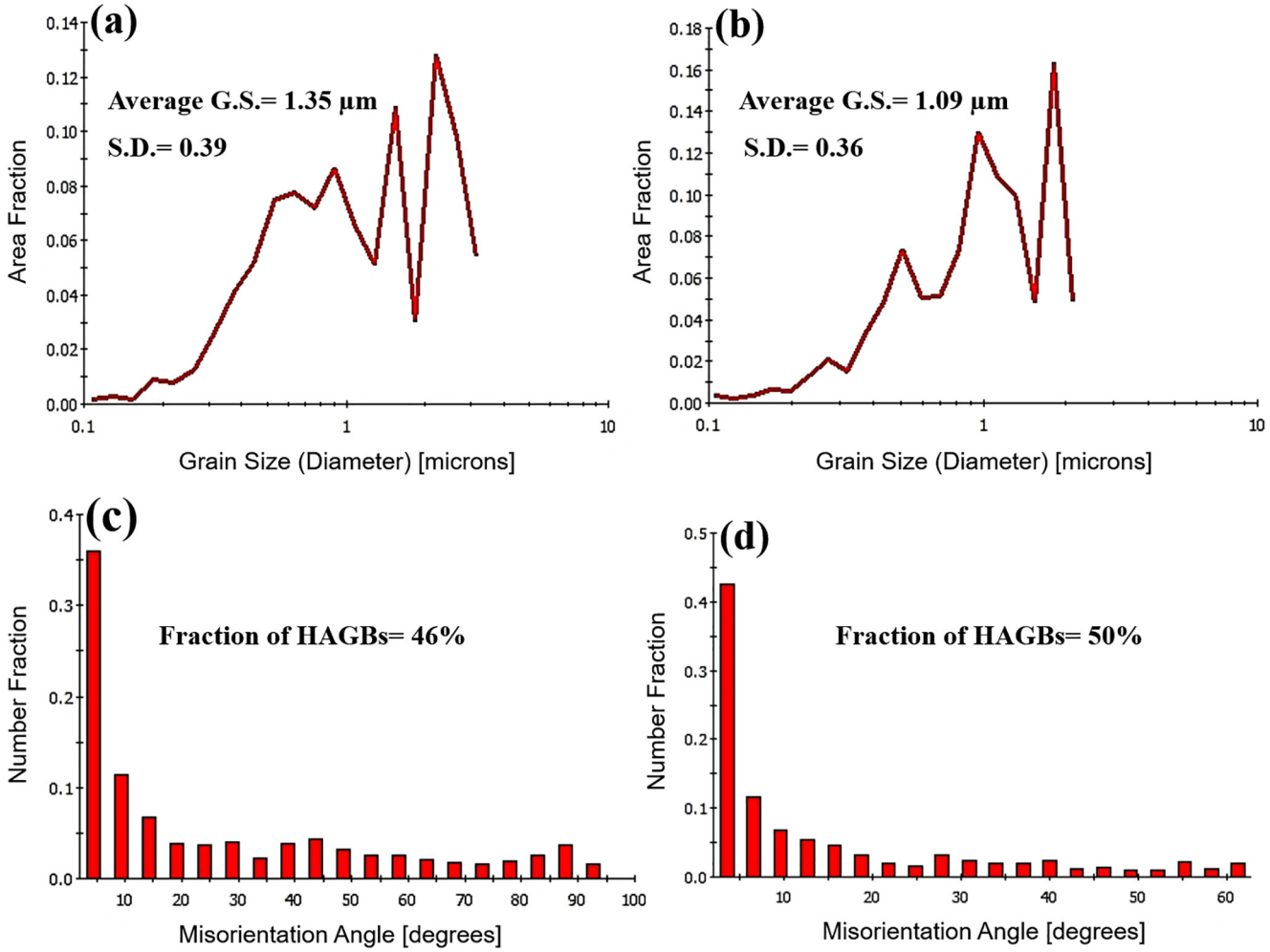

Fig. 5. The area fraction of grain size in CP titanium; (a) after the second pass, (b) after the fourth pass of ECAP passes. The misorientation distribution of CP titanium samples; (c) after the second pass, (d) after the four passes of ECAP process.

continuous dynamic recrystallization mechanism is higher in the four passes ECAPed sample as compared to two passes ECAPed counterpart. As reported in previous works, grain refinement of materials by ECAP technique is taken place under the generation of dislocations and twinnings and also, the increment of their density [31–33]. Then, the dense dislocation walls and dislocation tangles in the origin coarse grains are developed and transformed gradually into the boundaries with small misorientation angles which are called low angle grain boundaries (LAGBs). This phenomenon occurs through dynamic recovery and restoration mechanisms [31]. By further addition of pass numbers and increment of imposed plastic strains, the misorientation between various subgrains increases since the LAGBs are finally evolved to the HAGBs and eventually, grain refinement is attained. This process mainly progresses by continuous dynamic recrystallization phenomenon which is not unusual for titanium with high stacking fault energy [34,35]. Furthermore, the existence of second-phases, particles, and inclusions in the matrix of pure metals which possibly have higher hardness magnitudes could promote the dynamic recrystallization (DRX) phenomenon [36,37]. This occurrence is due to the activation of particle stimulated nucleation (PSN) mechanism. In titanium usually, carbides in the form of TiC_x are responsible for the PSN related DRX initiation. The second particle strengthening through carbide particles is achieved by impeding the dislocation motion in the matrix, also carbides can significantly affect the dislocation configuration during the deformation process, hence the second-phase must have an influence on the microstructural evolution during processing [38].

As mentioned before, electron back-scatter diffraction was implemented to characterize and evaluate the changes of grain refinements along with the ECAP pass numbers. As known [39], a homogenous structure formation of materials after applying different SPD processes may be attributed to the balance between the accumulation of dislocations and the reduction of stored energy by the migration of mobile grain boundaries which leads to softening through recovery. It seems that the addition of higher ECAP pass numbers leads to the increment of dislocations density. Since titanium has high stacking fault energy, it is prone to dynamic recovery. As a result, dislocations accumulation and their rearrangement lead to the dislocations tangles. Subsequently, by the initiation of a dynamic recovery mechanism, these dislocations rearrange in cell structures. The formation of cell structures may cause minimizing the total energy of the system. Consequently, after the fourth pass, it is difficult to further refine the material's structure due to the resistance of the ultrafine structure to more segmentation due to the large numbers of immobile dislocations and grain boundaries.

Additionally, the amount of HAGBs is enhanced to about 50% in the four passes sample and the grain size distribution of this sample shows a multimodal behavior. This means that in order to attain a more homogenous structure with a higher fraction of HAGBs, more ECAP passes should be utilized. However, according to the standard deviation magnitudes showing in Fig. 5(c) and (d), the four passes sample with the amount of 0.36 has a higher homogenous microstructure than the two passes counterpart with 0.39 standard deviation value. Therefore, it could be anticipated that the four passes sample may have more uniform mechanical behavior.

Mechanical properties

Fig. 6 describes the effect of ECAP pass numbers on shear yield strength, ultimate shear strength, and ductility. It can be seen that the ECAP process and addition of pass number lead to the improvement of material strength and decrement of ductility. For instance, both yield and ultimate shear strengths are respectively increased by 141% and 78%, while the ductility is decreased by almost 28% by the employment of four passes ECAP process as compared to the initial condition. As seen in Fig. 6, the mechanical properties especially the strength of pure Ti show no noticeable change from 2 to 4 passes. The additional pass

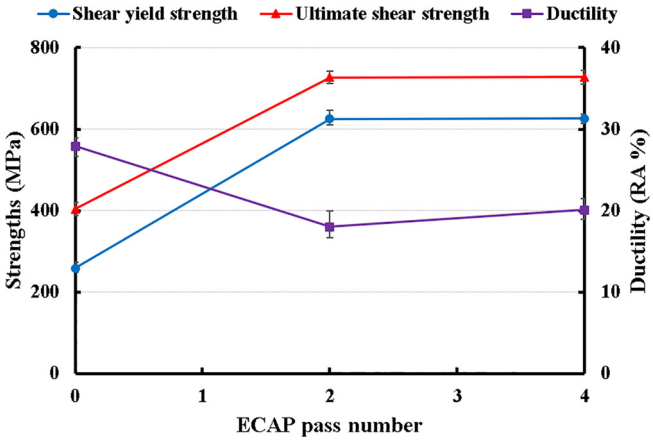

Fig. 6. Shear yield strength, ultimate shear strength, and ductility of CP titanium before and after the ECAP process up to four passes.

numbers not only cause more homogeneous hardness distribution but also leads to a more equiaxed structure [40]. Furthermore, the mean grain size does not change considerably in higher pass numbers compared to initial passes as reported in many investigations [40,41], hence by considering the Hall-Petch relationship [42], it can be expected that the strength and hardness magnitudes may present negligible difference in higher ECAP pass numbers. Moreover, improvement of the sample's ductility after the four passes as compared to the two passes is directly related to the transformation of LAGBs into HAGBs during the additional pass numbers of three and four. The EBSD analyses showed that the four-pass ECAPed titanium has more HAGBs as compared to the two-pass counterpart. The same results have been previously reported for the ECARed pure aluminum [43], ECAPed Al6061 [44], ECAPed Al7075 [45], HPTed pure copper [46], etc.

The average Vickers hardness (HV) magnitude as a function of the ECAP pass number is shown in Fig. 7. Accordingly, noticeable improvement of hardness is achieved after the first pass. Further ECAP processing results in a lower rate of hardness increment and finally, reaches the steady-state level at the final pass. The hardness magnitude reaches 249 HV after applying four ECAP passes. This corresponds to about 50% enhancement of hardness compared to the initial condition. As discussed above, it seems that the accumulation of plastic strains up to the fourth pass is the extent that the balance between dislocations and twinnings accumulation and grain boundaries migration is achieved. So, the structure is at the steady-state level and further improvement of mechanical properties using grain refinement would be very hard. The rapid improvement of hardness magnitude at the initial

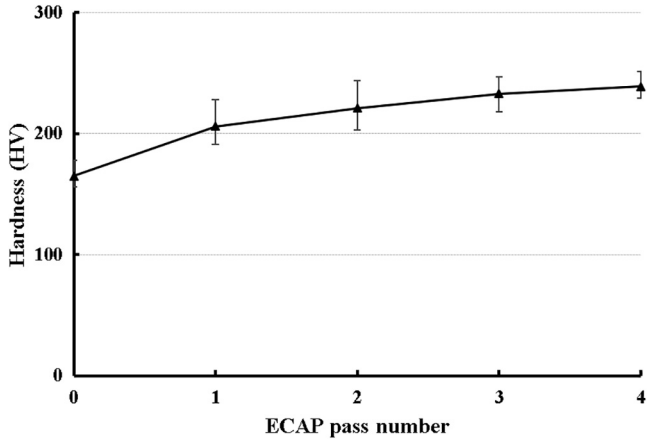

Fig. 7. Vickers hardness magnitude as a function of ECAP pass numbers for the CP titanium samples.

Table 2
Comparison of the enhancement of hardness for CP titanium due to ECAP processing with previous works.

Authors	Die channel angle (°)	Initial hardness (HV)	Hardness after four passes (HV)	Increasing rate (%)
Current work	90	166	249	50
Hajizadeh et al. [47]	90	202	265	31
Xiaoyan et al. [48]	90	155	256	65
Filho et al. [49]	90 (hot at 300 ℃)	145	229	58
	90 (hot & cold rolling)	236	271	15
Zhao et al. [50]	120	162	232	43

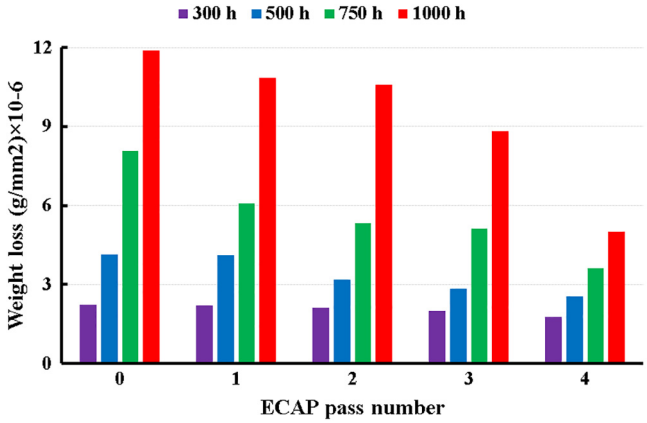

Fig. 8. Weight loss of initial and ECAP processed CP titanium after the erosion-corrosion experiment during a different time duration.

passes and reduction of its increasing trend at the subsequent passes have been previously reported. A comparison between the current and previous studies on the enhancement of hardness for CP titanium due to ECAP processing has been presented in Table 2.

Erosion-corrosion evaluation

The erosion-corrosion relates to an acceleration in the rate of corrosion attack in materials due to the mobility of corrosive fluid. In this work, erosion-corrosion resistance of CP titanium has been evaluated before and after the ECAP process up to the four passes using the weight loss per unit area. Fig. 8 has been obtained and plotted accordingly. It is found that erosion-corrosion of both initial and processed samples increases with the addition of time duration. Furthermore, the rate of erosion-corrosion decreases gradually by increasing the ECAP pass numbers. Consequently, the least weight loss magnitude (most resistant case) is observed for the CP titanium after the four ECAP passes irrespective of the time duration. It is noted that imposing the ECAP process and the addition of pass numbers result in improving the hardness of the CP titanium. Consequently, weight loss due to the erosion-corrosion decreases. Although considerable hardness increase has been obtained after the first ECAP pass number, substantial improvement in erosion-corrosion resistance is observed after the four passes of the ECAP process, this is attributed to material homogeneity which will be discussed later. Fig. 9 shows the EDS results of the ECAPed Ti sample after the erosion-corrosion test, as can be seen, the oxygen element existed on the sample, is an indication of TiO_2 formation. Also, the presence of other elements is the direct result of the sample's exposure to the simulated body fluids during the E-C experiment. The reduction of erosion-corrosion rate at the higher pass numbers occurs due to the enhanced strength of the sample caused by the strain-hardening through severe plastic deformation, the quick formation of the oxide layer (TiO_2) on the surface structure, and mighty bond layer with the surface. Similar results have been reported on the effect of time duration on erosion-corrosion of other ECAPed copper and aluminum materials [51].

Material homogeneity assessment

For evaluation of strain distribution at the initial and processed samples, hardness measurement at different positions along the cross-section and longitudinal planes of the specimens was performed as illustrated in Fig. 2(a). In this regard, a factor entitled hardness homogeneity index (HHI) has been employed based on the standard deviation to assess the hardness uniformity of the ECAPed samples [52,53]. The relationship of hardness homogeneity index is as follow:

$$HHI = \sqrt{\frac{\sum_{N}^{i=1} (HV_i - \overline{HV})^2}{N - 1}} \quad (1)$$

The HV is the individual Vickers hardness magnitude, N is the number of data points, and $\overline{HV}$ is the mean value of all measured hardness values. Tables 3 and 4 list the HV magnitudes and their homogeneity index before and after the ECAP process up to the four passes. Obviously, the hardness magnitude near the sample's surface is higher than that of the center of cross-section. This is due to the friction effect between the outer surfaces of the sample and the inner walls of the die. For example, the hardness variation between point 1 and point 3 (Fig. 2(a)) is about 3% for the as-received annealed titanium sample. Moreover, hardness results of the cross-section indicated that the sample before ECAP processing has the least HHI with a magnitude of 3.2. It means that it possesses the most homogeneous structure. After the application of one pass ECAP, the HHI magnitude increases to 5.3 which is about 65% higher than that of the initial condition. Also, the second pass CP titanium exhibits the highest magnitude of HHI with 17% higher than the first pass counterpart. At the higher pass numbers, the HHI magnitude begins to decrease in which the third and fourth passes of the ECAP process lead to the reduction of HHI having respectively the magnitudes of 5.2 and 4.2. Thus, initial pass numbers are so important at the increment of HV magnitude, while the subsequent ones lead to the uniform distribution of hardness. The same trend is also observed for the hardness homogeneity index on the longitudinal plane. It should be noted that the results of hardness homogeneity correspond to a rational uniformity at the microstructure of the material.

Overall, the hardness homogeneity index as a measure of hardness uniformity (strain or residual stress uniformity) obtained at different positions shows that the fourth pass ECAPed sample exhibits a better homogeneity as compared to the other passes. Although the average hardness magnitude is increased by about 47% by imposing four ECAP passes, its uniformity is only reduced by 17%. Therefore, better homogeneity of the material is achieved throughout the longitudinal and cross-sectional directions of titanium sample as the number of ECAP passes increases to four passes. As discussed before, Fig. 8 shows significant improvement in the erosion-corrosion resistance of CP titanium after the four passes of the ECAP process, this is associated with the material homogeneity.

The other significant matter is related to the formation of the oxide layer on the surface which resists corrosive attack. ECAP process leads to the production of titanium with a high density of grain boundaries, twinnings, and dislocations inside the origin grains which can be suitable sites for the nucleation of the passive film. Consequently, the passivation layer of the processed sample is formed faster and the

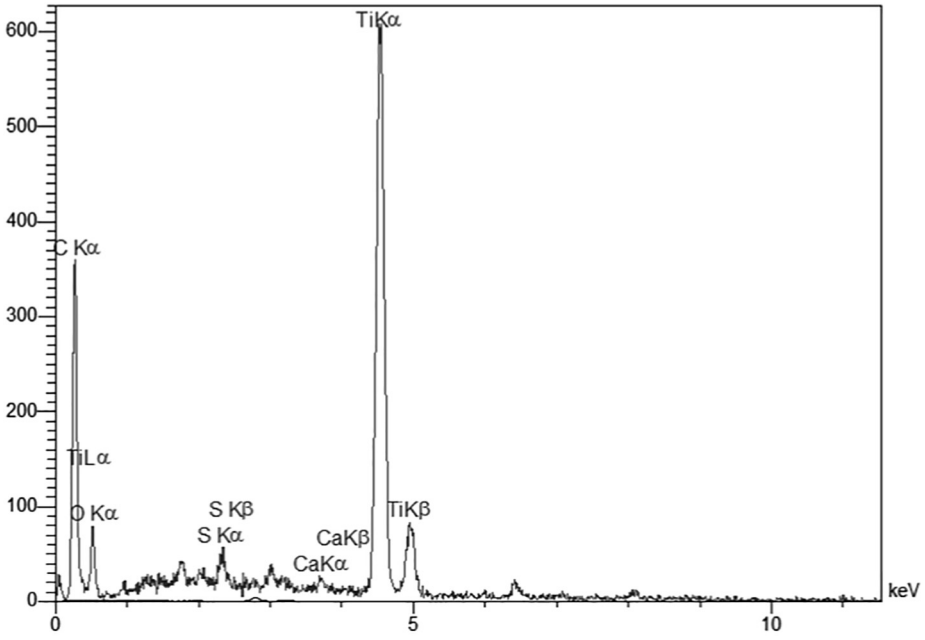

Fig. 9. EDS results of the ECAPed Ti after imposing four passes showing the formation of TiO_2.

Table 3
Vickers hardness magnitude and its homogeneity index along the cross-section of CP titanium before and after the ECAP process up to four passes.

Position/Condition	Initial condition	ECAP process up to			
		Pass 1	Pass 2	Pass 3	Pass 4
1	173	210	222	240	246
2	169	209	223	232	251
3	168	204	226	238	249
4	170	203	217	232	250
5	173	208	218	243	247
6	175	216	227	242	255
7	174	214	224	241	250
8	168	208	211	231	242
9	166	199	210	230	242
Average magnitude	170.7	207.9	219.8	236.5	248
Hardness homogeneity index	3.2	5.3	6.2	5.2	4.2

bonding strength of the oxide layer to the surface is stronger as compared to the initial material. If the oxide layer is damaged by the action of erosion, the repair of the passive layer occurs faster; hence, the rate of erosion-corrosion is diminished. In addition to this phenomenon, it should be considered that CP titanium with the highest homogeneity (final pass ECAPed condition) is the most resistant to surface degradation. The enhancement of hardness and its homogeneity possibly is favorable to reduce the synergism rate and the higher relative wear resistance of the material which in turn affects the erosion-corrosion behavior [54]. It was found that the hardness of the surface is inversely proportional to erosion rate [55], in another study [56], it was reported that increasing hardness of surface leads to the improved E-C rate. Also, the existence of residual stress in hard-to-deform materials could be another possible reason which would activate the brittle cracking of the erosive wear [56,57].

Conclusions

This work deals with ECAP processing of CP titanium up to four passes and its effect on the microstructure, mechanical, and tribological properties. Also, the role of the material homogeneity on the behavior of processed samples was evaluated. The following conclusions are made from the current study:

- Commercial pure titanium was successfully processed up to four

Table 4
Vickers hardness magnitude and its homogeneity along the longitudinal of CP titanium before and after the ECAP process up to four passes.

Position/Condition	Initial condition	ECAP process up to			
		Pass 1	Pass 2	Pass 3	Pass 4
1/1′/1″	173/169/164	211/204/198	227/225/220	241/238/231	255/251/244
2/2′/2″	173/167/165	210/210/196	229/224/217	245/233/230	254/247/247
3/3′/3″	170/166/166	215/210/199	227/220/219	242/235/231	255/250/246
4/4′/4″	174/169/163	209/209/200	225/220/215	238/240/229	256/246/247
5/5′/5″	173/166/166	209/207/200	223/219/216	240/235/236	252/252/244
6/6′/6″	172/165/162	208/202/196	229/222/214	242/239/236	253/249/245
7/7′/7″	170/170/161	213/207/201	230/219/216	241/235/235	253/245/244
8/8′/8″	172/167/162	209/205/198	228/219/215	241/236/237	255/246/243
9/9′/9″	175/166/163	211/206/198	229/219/214	246/232/229	253/247/247
10/10′/10″	171/170/164	215/210/200	230/224/213	242/234/235	254/252/247
11/11″/11″	172/165/165	214/210/199	231/222/216	244/240/231	253/245/243
12/12′/12″	174/170/166	211/203/201	229/223/220	239/233/230	255/248/245
Average magnitude	167.9	205.7	221.9	236.7	249.1
Hardness homogeneity index	3.9	5.6	5.4	4.7	4.1

passes by ECAP die with the channel angle of 90°. Neither damage nor failure was observable on the samples after processing.

- The average grain size of the titanium sample after the second and fourth passes of the ECAP process is about 1.35 and 1.09 μm; however, there are a considerable number of ultrafine grains in the range of 400–500 nm and even many nanostructures with the order of 100 nm. Also, the addition of ECAP pass numbers increases the fraction of high angle grain boundaries.
- Results of the torsion test indicated that the yield and ultimate shear strengths are respectively increased by 141% and 78% while the ductility of the material is decreased by 28% after imposing four passes as compared to the as-received condition. Also, improving its ductility at the final pass as compared to the initial passes is related to the transformation of some LAGBs into HAGBs.
- Hardness measurements represented that noticeable improvement of hardness is attained after the first pass. Moreover, the growth rate of hardness is gradually reduced by further ECAP processing and eventually, reached the steady-state level at the final pass. At this condition, the balance between dislocations and twinnings accumulation and grain boundaries migration is achieved. Thus, a uniform hardness distribution on both the cross-sectional and longitudinal planes is seen.
- The erosion-corrosion resistance of processed samples is improved by a combination of a) grain refinement, b) material homogeneity, and c) quick formation and a strong bond layer of the oxide layer (TiO_2) to the surface.

CRediT authorship contribution statement

Sh. Attarilar: Data curation, Writing - review & editing. **F. Djavanroodi:** Conceptualization, Funding acquisition, Resources. **O.M. Irfan:** Visualization, Investigation. **F.A. Al-Mufadi:** Software, Methodology. **M. Ebrahimi:** Data curation, Formal analysis, Conceptualization, Writing - original draft. **Q.D. Wang:** Writing - review & editing.

Declaration of Competing Interest

The authors declare that they have no known competing financial interests or personal relationships that could have appeared to influence the work reported in this paper.

Acknowledgments

The authors would like to acknowledge the support received from King Abdul-Aziz City for Science and Technology (KACST) for funding this work under the grant number of 35-89. Also, the support provided by the Engineering College, Qassim University is gratefully acknowledged.

Data availability

All data generated or analyzed during this study are included in this published article.

References

[1] Balyanov A, Kutnyakova J, Amirkhanova NA, Stolyarov VV, Valiev RZ, Liao XZ, et al. Corrosion resistance of ultra fine-grained Ti. Scr Mater 2004;51:225–9. https://doi.org/10.1016/j.scriptamat.2004.04.011.

[2] Zhang ZJ, Son IH, Im YT, Park JK. Finite element analysis of plastic deformation of CP-Ti by multi-pass equal channel angular extrusion at medium hot-working temperature. Mater Sci Eng, A 2007;447:134–41. https://doi.org/10.1016/j.msea.2006.10.068.

[3] Gangwar K, Ramulu M. Friction stir welding of titanium alloys: a review. Mater Des 2018;141:230–55. https://doi.org/10.1016/j.matdes.2017.12.033.

[4] Zhang LC, Chen LY, Wang L. Surface modification of titanium and titanium alloys: technologies, developments, and future interests. Adv Eng Mater 2020;1901258:1–37. https://doi.org/10.1002/adem.201901258.

[5] Hafeez N, Liu S, Lu E, Wang L, Liu R, Lu W, Zhang LC. Mechanical behavior and phase transformation of β-type Ti-35Nb-2Ta-3Zr alloy fabricated by 3D-Printing. J. Alloys Compd. 2019;790:117–26. https://doi.org/10.1016/j.jallcom.2019.03.138.

[6] Liu S, Liu J, Wang L, Ma RLW, Zhong Y, Lu W, et al. Superelastic behavior of in-situ eutectic-reaction manufactured high strength 3D porous NiTi-Nb scaffold. Scr Mater 2020;181:121–6. https://doi.org/10.1016/j.scriptamat.2020.02.025.

[7] Gurrappa I. Characterization of titanium alloy Ti-6Al-4V for chemical, marine and industrial applications. Mater Charact 2003;51:131–9. https://doi.org/10.1016/j.matchar.2003.10.006.

[8] Zhang ZX, Qu SJ, Feng AH, Shen J. Achieving grain refinement and enhanced mechanical properties in Ti–6Al–4V alloy produced by multidirectional isothermal forging. Mater Sci Eng, A 2017;692:127–38. https://doi.org/10.1016/j.msea.2017.03.024.

[9] Valiev RZ, Langdon TG. Principles of equal-channel angular pressing as a processing tool for grain refinement. Prog Mater Sci 2006;51:881–981. https://doi.org/10.1016/j.pmatsci.2006.02.003.

[10] Cherukuri B, Nedkova TS, Srinivasan R. A comparison of the properties of SPD-processed AA-6061 by equal-channel angular pressing, multi-axial compressions/forgings and accumulative roll bonding. Mater Sci Eng, A 2005;410–411:394–7. https://doi.org/10.1016/j.msea.2005.08.024.

[11] Djavanroodi F, Ebrahimi M. Effect of die channel angle, friction and back pressure in the equal channel angular pressing using 3D finite element simulation. Mater Sci Eng, A 2010;527:1230–5. https://doi.org/10.1016/j.msea.2009.09.052.

[12] Khereddine AY, Larbi FH, Kawasaki M, Baudin T, Bradai D, Langdon TG. An examination of microstructural evolution in a Cu-Ni-Si alloy processed by HPT and ECAP. Mater Sci Eng, A 2013;576:149–55. https://doi.org/10.1016/j.msea.2013.04.004.

[13] Ebrahimi M, Shamsborhan M. Monotonic and dynamic mechanical properties of PTCAE aluminum. J Alloy Compd 2017;705:28–37. https://doi.org/10.1016/j.jallcom.2017.02.109.

[14] Shamsborhan M, Ebrahimi M. Production of nanostructure copper by planar twist channel angular extrusion process. J Alloy Compd 2016;682:552–6. https://doi.org/10.1016/j.jallcom.2016.05.012.

[15] Ebrahimi M, Attarilar S, Djavanroodi F, Gode C, Kim HS. Wear properties of brass samples subjected to constrained groove pressing process. Mater Des 2014;63:531–7. https://doi.org/10.1016/j.matdes.2014.06.043.

[16] Djavanroodi F, Ebrahimi M, Nayfeh JF. Tribological and mechanical investigation of multi-directional forged nickel. Sci Rep 2019:1–8. https://doi.org/10.1038/s41598-018-36584-w.

[17] Ebrahimi M, Gholipour H, Djavanroodi F. A study on the capability of equal channel forward extrusion process. Mater Sci Eng, A 2015;650:1–7. https://doi.org/10.1016/j.msea.2015.10.014.

[18] Ebrahimi M, Par MA. Twenty-year uninterrupted endeavor of friction stir processing by focusing on copper and its alloys. J Alloy Compd 2019;781:1074–90. https://doi.org/10.1016/j.jallcom.2018.12.083.

[19] Beygelzimer Y, Varyukhin V, Synkov S, Orlov D. Useful properties of twist extrusion. Mater Sci Eng, A 2009;503:14–7. https://doi.org/10.1016/j.msea.2007.12.055.

[20] Hosseini SA, Manesh HD. High-strength, high-conductivity ultra-fine grains commercial pure copper produced by ARB process. Mater Des 2009;30:2911–8. https://doi.org/10.1016/j.matdes.2009.01.012.

[21] Richert M, Stüwe HP, Zehetbauer MJ, Richert J, Pippan R, Motz C, et al. Work hardening and microstructure of AlMg5 after severe plastic deformation by cyclic extrusion and compression. Mater Sci Eng, A 2003;355:180–5. https://doi.org/10.1016/S0921-5093(03)00046-7.

[22] Xun Y, Mohamed FA. Refining efficiency and capability of top-down synthesis of nanocrystalline materials. Mater Sci Eng A 2011;528:5446–52. https://doi.org/10.1016/j.msea.2011.03.015.

[23] Wang L, Xie L, Lv Y, Zhang LC, Chen L, Meng Q, et al. Microstructure evolution and superelastic behavior in Ti-35Nb-2Ta-3Zr alloy processed by friction stir processing. Acta Mater 2017;131:499–510. https://doi.org/10.1016/j.actamat.2017.03.079.

[24] Djavanroodi F, Ebrahimi M. Effect of die parameters and material properties in ECAP with parallel channels. Mater Sci Eng, A 2010;527:7593–9. https://doi.org/10.1016/j.msea.2010.08.022.

[25] Djavanroodi F, Ebrahimi M, Rajabifar B, Akramizadeh S. Fatigue design factors for ECAPed materials. Mater Sci Eng, A 2010;528:745–50. https://doi.org/10.1016/j.msea.2010.09.080.

[26] Ebrahimi M, Shaeri MH, Gode C, Armoon H, Shamsborhan M. The synergistic effect of dilute alloying and nanostructuring of copper on the improvement of mechanical and tribological response. Compos Part B Eng 2019;164:508–16. https://doi.org/10.1016/j.compositesb.2019.01.077.

[27] Irfan OM, Al-Mufadi FA, Djavanroodi F. Surface Properties and Erosion-Corrosion Behavior of Nanostructured Pure Titanium in Simulated Body. Fluid Metall Mater Trans A Phys Metall Mater Sci 2018;49:5695–704. https://doi.org/10.1007/s11661-018-4837-3.

[28] Panigrahi A, Bönisch M, Waitz T, Schafler E, Calin M, Eckert J, et al. Phase transformations and mechanical properties of biocompatible Ti-16.1Nb processed by severe plastic deformation. J Alloys Compd 2015;628:434–41. https://doi.org/10.1016/j.jallcom.2014.12.159.

[29] Selvam K, Mandal P, Grewal HS, Arora HS. Ultrasonic cavitation erosion-corrosion behavior of friction stir processed stainless steel. Ultrason Sonochem 2018;44:331–9. https://doi.org/10.1016/j.ultsonch.2018.02.041.

[30] Ortiz-Cuellar E, Hernandez-Rodriguez MAL, García-Sanchez E. Evaluation of the tribological properties of an Al-Mg-Si alloy processed by severe plastic deformation. Wear 2011;271:1828–32. https://doi.org/10.1016/j.wear.2010.12.082.

[31] Sakai T, Belyakov A, Kaibyshev R, Miura H, Jonas JJ. Dynamic and post-dynamic recrystallization under hot, cold and severe plastic deformation conditions. Prog Mater Sci 2014;60:130–207. https://doi.org/10.1016/j.pmatsci.2013.09.002.
[32] Ansarian I, Shaeri MH, Ebrahimi M, Minárik P, Bartha K. Microstructure evolution and mechanical behaviour of severely deformed pure titanium through multi directional forging. J Alloy Compd 2019;776:83–95. https://doi.org/10.1016/j.jallcom.2018.10.196.
[33] Tolaminejad B, Dehghani K. Microstructural characterization and mechanical properties of nanostructured AA1070 aluminum after equal channel angular extrusion. Mater Des 2012;34:285–92. https://doi.org/10.1016/j.matdes.2011.08.003.
[34] Humphreys FJ, Hatherly M. Recrystallization and Related Annealing Phenomena, 2th ed., Elsevier Ltd., 2004. https://doi.org/10.1017/CBO9781107415324.004.
[35] Attarilar S, Salehi MT, Al-Fadhalah KJ, Djavanroodi F, Mozafari M. Functionally graded titanium implants: Characteristic enhancement induced by combined severe plastic deformation. PLoS One 2019;14:1–18. https://doi.org/10.1371/journal.pone.0221491.
[36] Huang K, Logé RE. A review of dynamic recrystallization phenomena in metallic materials. Mater Des 2016;111:548–74. https://doi.org/10.1016/j.matdes.2016.09.012.
[37] Liu H, Ju J, Yang X, Yan J, Song D, Jiang J, et al. A two-step dynamic recrystallization induced by LPSO phases and its impact on mechanical property of severe plastic deformation processed Mg97Y2Zn1alloy. J Alloy Compd 2017;704:509–17. https://doi.org/10.1016/j.jallcom.2017.02.107.
[38] Zhang S, Zeng W, Gao X, Zhou D, Lai Y. Role of titanium carbides on microstructural evolution of Ti-35V-15Cr-0.3Si-0.1C alloy during hot working. J. Alloys Compd. 2016;684:201–10. https://doi.org/10.1016/j.jallcom.2016.05.176.
[39] Matsunoshita H, Edalati K, Furui M, Horita Z. Materials Science & Engineering A Ultra fi ne-grained magnesium – lithium alloy processed by high- pressure torsion : Low-temperature superplasticity and potential for hydroforming. Mater Sci Eng, A 2015;640:443–8. https://doi.org/10.1016/j.msea.2015.05.103.
[40] Mishra A, Richard V, Grégori F, Asaro RJ, Meyers MA. Microstructural evolution in copper processed by severe plastic deformation. Mater Sci Eng, A 2005;410–411:290–8. https://doi.org/10.1016/j.msea.2005.08.201.
[41] Attarilar S, Salehi MT, Djavanroodi F. Microhardness evolution of pure titanium deformed by equal channel angular extrusion. Metall Res Technol 2019;116. https://doi.org/10.1051/metal/2018135.
[42] Pande CS, Cooper KP. Progress in Materials Science Nanomechanics of Hall – Petch relationship in nanocrystalline materials. Prog Mater Sci 2009;54:689–706. https://doi.org/10.1016/j.pmatsci.2009.03.008.
[43] Azimi A, Tutunchilar S, Faraji G, Besharati Givi MK. Mechanical properties and microstructural evolution during multi-pass ECAR of Al 1100-O alloy. Mater Des 2012;42:388–94. https://doi.org/10.1016/j.matdes.2012.06.035.
[44] Horita Z, Fujinami T, Nemoto M, Langdon TG. Improvement of mechanical properties for Al alloys using equal-channel angular pressing. J Mater Process Technol 2001;117:288–92. https://doi.org/10.1016/S0924-0136(01)00783-X.
[45] Shaeri MH, Shaeri M, Salehi MT, Seyyedein SH, Abutalebi MR. Effect of equal channel angular pressing on aging treatment of Al-7075 alloy. Prog Nat Sci Mater Int 2015;25:159–68. https://doi.org/10.1016/j.pnsc.2015.03.005.
[46] Alawadhi MY, Sabbaghianrad S, Huang Y, Langdon TG. Direct influence of recovery behaviour on mechanical properties in oxygen-free copper processed using different SPD techniques: HPT and ECAP. J Mater Res Technol 2017;6:369–77. https://doi.org/10.1016/j.jmrt.2017.05.005.
[47] Hajizadeh K, Eghbali B, Topolski K, Kurzydlowski KJ. Ultra-fine grained bulk CP-Ti processed by multi-pass ECAP at warm deformation region. Mater Chem Phys 2014;143:1032–8. https://doi.org/10.1016/j.matchemphys.2013.11.001.
[48] Liu X, Zhao X, Yang X, Jia J, Qi B. The evolution of hardness homogeneity in commercially pure Ti processed by ECAP. J Wuhan Univ Technol Mater Sci Ed 2014;29:578–84. https://doi.org/10.1007/s11595-014-0960-1.
[49] Mendes Filho AA, Rovere CA, Kuri SE, Sordi VL, Ferrante M. A general study of commercially pure Ti subjected to severe plastic deformation: Microstructure, strength and corrosion resistance. Rev Mater 2010;15:286–92.
[50] Zhao X, Fu W, Yang X, Langdon TG. Microstructure and properties of pure titanium processed by equal-channel angular pressing at room temperature. Scr Mater 2008;59:542–5. https://doi.org/10.1016/j.scriptamat.2008.05.001.
[51] Irfan OM, Al-mufadi F, Al-shataif Y, Djavanroodi F. Effect of Equal Channel Angular Pressing (ECAP) on Erosion-Corrosion of Pure Copper. Appl Sci 2017;7:1–17. https://doi.org/10.3390/app7121250.
[52] Lee HJ, Ahn B, Kawasaki M, Langdon TG. Evolution in hardness and microstructure of ZK60A magnesium alloy processed by high-pressure torsion. J Mater ResTechnol. 2015;4:18–25. https://doi.org/10.1016/j.jmrt.2014.10.015.
[53] Djavanroodi F, Omranpour B, Ebrahimi M, Sedighi M. Progress in Natural Science : Materials International Designing of ECAP parameters based on strain distribution uniformity. Prog Nat Sci Mater Int 2012;22:452–60. https://doi.org/10.1016/j.pnsc.2012.08.001.
[54] Xiulin Ji LG, Zhao Jianhua, Yang Shunzhen. Erosion-corrosion behavior of electrodeposited amorphous Ni-W-P coating in saline-sand slurry. Corrosion 2013;69:593–600. https://doi.org/10.1016/j.matdes.2016.04.004.
[55] Hutchings IM. Tribology, friction and wear of engineering materials Elsevier; 1992. https://doi.org/10.1016/j.msea.2014.10.030.
[56] Lotfollahi M, Shamanian M, Saatchi A. Effect of friction stir processing on erosion-corrosion behavior of nickel-aluminum bronze. Mater Des 2014;62:282–7. https://doi.org/10.1016/j.matdes.2014.05.037.
[57] Prevey PS, Hombach DJ, Jayaraman N. Controlled plasticity burnishing to improve the performance of friction stir processed Ni-Al bronze. Mater Sci Forum 2007;539–543:3807–13. https://doi.org/10.4028/www.scientific.net/msf.539-543.3807.